

# Coupled CFD-FEM simulation of hydrodynamic responses of a CALM buoy

Haoyuan Gu<sup>\*1</sup>, Hamn-Ching Chen<sup>2</sup> and Linyue Zhao<sup>3</sup>

<sup>1</sup>Department of Civil Engineering, Texas A&M University, College Station, Texas, USA

<sup>2</sup>Zachry Department of Civil Engineering and Department of Ocean Engineering, College Station, Texas, USA

<sup>3</sup>Saipem America Inc., Houston, Texas, USA

(Received December 9, 2018, Revised February 9, 2019, Accepted February 16, 2019)

**Abstract.** In this paper, the Finite-Analytic Navier-Stokes (FANS) code is coupled with an in-house finite-element code to study the dynamic interaction between a floating buoy and its mooring system. Hydrodynamic loads on the buoy are predicted with the FANS module, in which Large Eddy Simulation (LES) is used as the turbulence model. The mooring lines are modeled based on a slender body theory. Their dynamic responses are simulated with a nonlinear finite element module, MOORING3D. The two modules are coupled by transferring the forces and displacements of the buoy and its mooring system at their connections through an interface module. A free-decay model test was used to calibrate the coupled method. In addition, to investigate the capability of the present coupled method, numerical simulations of two degree-of-freedom vortex-induced motion of a CALM buoy in uniform currents were performed. With the study it can be verified that accurate predictions of the motion responses and tension responses of the CALM buoy system can be made with the coupling CFD-FEM method.

**Keywords:** Catenary Anchor Leg Mooring (CALM) buoy system; computational fluid dynamics (CFD); unsteady Navier-Stokes equations; coupling mooring analysis; Large Eddy Simulation (LES)

## 1. Introduction

The dynamic behavior of the catenary anchor leg mooring (CALM) system has been a subject of study for a long time since it was first employed in 1961. As the hydrodynamic behavior of the CALM buoy is highly affected by the mooring system dynamics, an accurate tool for coupled analysis is essential.

Many model tests have been performed by, among others, Bunnik *et al.* (2002), Ricbourg *et al.* (2006) to estimate the hydrodynamic behavior of CALM buoy models. The size of the buoy is scaled down based on Froude scaling law. Due to limited water depth in the wave basin, a method of equivalent truncated mooring system is applied for deep water prototypes.

In terms of numerical analysis, many coupled studies have been conducted based on diffraction/radiation theory, such as those presented by Kang *et al.* (2014), Huang *et al.* (2005), Le Cunff *et al.* (2007). They performed forced oscillation tests to validate hydrodynamic performance of buoy. Free-decay test is commonly employed to predict the performance of CALM buoy system,

---

\*Corresponding author, Ph.D. Student, E-mail: [hygu@tamu.edu](mailto:hygu@tamu.edu)

including the buoy model and offloading systems (Duggal and Ryu 2005, Salem *et al.* 2012). Different models are applied to simulate mooring line systems numerically, such as lumped mass method by Bunnik *et al.* (2002) and nonlinear springs replacement method by Sagrilo *et al.* (2002). Both fully-dynamic coupled method and quasi-static coupled method are commonly used to simulate the interaction between the floater and mooring system (Cozijn and Bunnik 2004).

In addition, CFD approach is also used to study the hydrodynamic behavior of the CALM buoy. Monroy *et al.* (2011) conducted CFD simulations of a captive CALM buoy with Reynolds Averaged Navier-Stokes Equations (RANSE) solver. The buoy model was kept captive by a framed structure without the coupling effect of the mooring system. Strong viscous effects such as vortex shedding was observed in the study. Gu *et al.* (2017) considered the dynamic interaction between a buoy model and its mooring lines by coupling the methods of CFD and FEM.

Gu *et al.* (2017) modeled the mooring system as catenary cables to provide similar hydrodynamic performance as the CALM system modeled in the free-decay test conducted by Ryu *et al.* (2006). As the method of equivalent truncated mooring system was employed in the model test, to facilitate a more direct comparison with the model test data, this paper replaced the imaginary catenary mooring system with a taut mooring system, whose parameters are the same as the ones provided by Ryu *et al.* (2006). The new CALM buoy system was calibrated with the free-decay test. The hydrodynamic behavior of the CALM buoy system was further investigated under the condition of uniform currents with different velocities.

In this study, the hydrodynamic responses of the floating buoy are predicted based on the FANS module. The mooring system is modeled and simulated with MOORING3D. Interactions between the buoy and its mooring system are considered through the interface module.

## 2. Numerical approach

### 2.1 MOORING3D

#### 2.1.1 Background

MOORING3D is a cable dynamic analysis Fortran 90 code developed by the authors. It is based on the nonlinear Finite Element Method (FEM) theory originally introduced by Garrett (1982). The theory is modified for the purpose of this research to couple with the FANS code.

In this study, the mooring system is modeled as long slender wires neglecting bending moments and shear forces. The primary force is the tension along the direction of wire. Based on the motion equation of a cable in Cartesian coordinate (Lindahl and Sjoberg 1983), the governing equation describing the motion of a cable can be expressed as

$$(\tilde{\lambda}\mathbf{r}')' + \mathbf{q} = \rho\ddot{\mathbf{r}} \quad (1)$$

$$\tilde{\lambda} = \frac{T}{1+\varepsilon} \quad (2)$$

$$\varepsilon = \frac{T}{EA} \quad (3)$$

where  $T$  is the tension tangential to wire's direction.  $\mathbf{r}$  is a function of both deformed arc length  $s$  and time  $t$ .  $\mathbf{q}$  is the external force per unit length.

For the  $\mathbf{q}$  considered here, it is composed of hydrostatic, hydrodynamic and gravity forces. The gravity force is determined by

$$\mathbf{q}_t(s, t) = -\rho_t g A_t \mathbf{e}_y \quad (4)$$

By considering the components of external force, we can express the governing equation as

$$\mathbf{M}\ddot{\mathbf{r}} - (\tilde{\lambda}\mathbf{r}')' = \mathbf{q} \quad (5)$$

where

$$\mathbf{M} = \rho_t A_t \mathbf{I} + \rho_f A_f C_{Mn} (1 + \varepsilon) \mathbf{N} + \rho_f A_f C_{Mt} (1 + \varepsilon) \mathbf{T} \quad (6)$$

$$\begin{aligned} \mathbf{q} = & (\rho_f A_f - \rho_t A_t) g \mathbf{e}_y + \rho_f A_f (1 + \varepsilon) (\mathbf{I} + C_{Mn} \mathbf{N} + C_{Mt} \mathbf{T}) \mathbf{a}_f + \frac{1}{2} \rho_f D_f C_{Dn} \\ & (1 + \varepsilon) \mathbf{N} (\mathbf{v}_f - \dot{\mathbf{r}}) |\mathbf{N} (\mathbf{v}_f - \dot{\mathbf{r}})| + \frac{1}{2} \rho_f D_f C_{Dt} (1 + \varepsilon) \mathbf{T} (\mathbf{v}_f - \dot{\mathbf{r}}) |\mathbf{T} (\mathbf{v}_f - \dot{\mathbf{r}})| \end{aligned} \quad (7)$$

$$\mathbf{T} = \frac{\mathbf{r}'^T \mathbf{r}'}{(1 + \varepsilon)^2} \quad (8)$$

In the above equations,  $A_t$  is the structural cross-section area of the rod.  $\rho_t$  is the density of the rod.  $\rho_f$  is the density of the water.  $A_f$  is the outer cross-section area of the rod.  $\mathbf{T}$  and  $\mathbf{N}$  are transfer matrices between the local coordinate system of the rod and global coordinate system.  $C_{Mn}$  is the normal added-mass coefficient.  $C_{Mt}$  is the tangential added-mass coefficient.  $C_{Dn}$  is the normal drag coefficient.  $C_{Dt}$  is the tangential drag coefficient.

The configuration vector  $\mathbf{r}$  must obey the stretching constrain equation

$$\mathbf{r}' \cdot \mathbf{r}' (1 - \tilde{\varepsilon})^2 = 1 \quad (9)$$

By employing Galerkin's method to discretize the partial differential terms and Hermite cubics  $a_i(\xi)$ /quadratics  $p_m(\xi)$  shape functions to discretize the coefficients in summation form, Eqs. (5) and (9) become

$$\gamma_{ikm} M_{njm} \ddot{u}_{kj} + \beta_{ikm} \tilde{\lambda}_m u_{kn} = \mu_{im} q_{mn} + f_{in} \quad (10)$$

$$\frac{1}{2} \beta_{ikm} u_{in} u_{kn} + \frac{1}{2} \tilde{\eta}_{iklm} (-2\tilde{\varepsilon}_l + \tilde{\varepsilon}_l^2) u_{in} u_{kn} - \frac{1}{2} \tau_m = 0 \quad (11)$$

where

$$\beta_{ikm} = \frac{1}{L} \int_0^1 a_i'(\xi) a_k'(\xi) p_m(\xi) d\xi \quad (12)$$

$$\gamma_{ikm} = L \int_0^1 a_i(\xi) a_k(\xi) p_m(\xi) d\xi \quad (13)$$

$$\mu_{im} = L \int_0^1 a_i(\xi) p_m(\xi) d\xi \quad (14)$$

$$\tilde{\eta}_{iklm} = \frac{1}{L} \int_0^1 a_i'(\xi) a_k'(\xi) p_l(\xi) p_m(\xi) d\xi \quad (15)$$

The unknown variables in Eqs. (10) and (11) are  $\ddot{u}_{kj}$ ,  $u_{kn}$  and  $\tilde{\lambda}_m$ , where  $j$ ,  $m$  and  $n$  are integers from 1 to 3 and  $i$ ,  $k$  are integers from 1 to 4. By considering the boundary conditions, we can write the equations in a matrix form of  $\mathbf{A}\delta\mathbf{x} = \mathbf{b}$ . The size of the matrix is determined by the number of segments in the line model. For more detailed information about the theory, please

refer to Chen (2002).

To evaluate the accuracy of the MOORING3D code, a prescribed motion test is conducted. The test's results are compared with the results from commercial software OrcaFlex under the same experimental condition.

### 2.1.2 Verification

The verification test consists of a 4-leg 90° spaced mooring lines. The 3D overview of the experimental set-up is shown in Fig. 1. The parameters of the four mooring lines are shown in Table 1. The top-end points of the mooring lines are attached to a buoy with coordinates of (8.5, 0), (0, 8.5), (0, -8.5), (-8.5, 0). The bottom-end points of the mooring lines are anchored on the sea floor with coordinates of (330, 0), (0, 330), (0, -330) and (-330, 0).

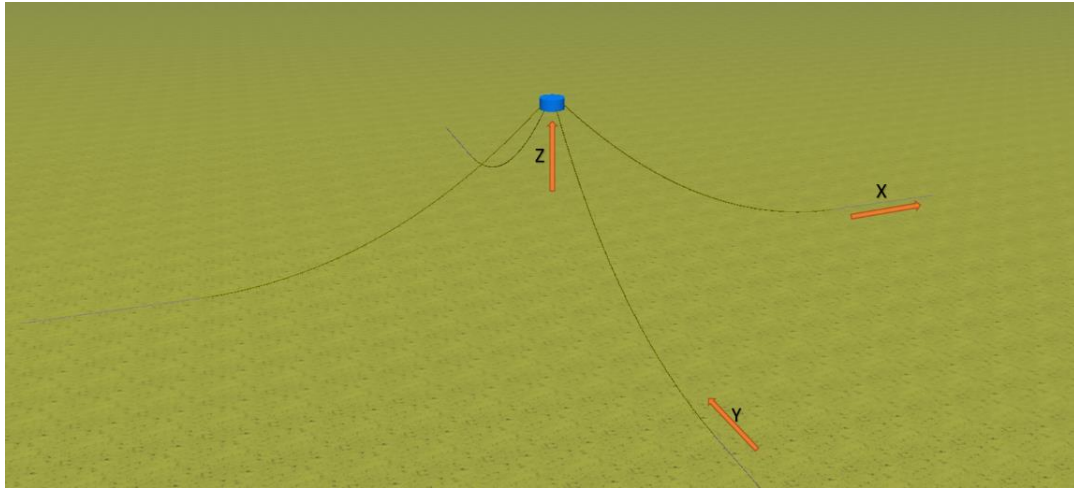


Fig. 1 3D overview of catenary mooring lines' configuration in the free-decay test

Table 1 Parameters of mooring lines in verification test

	Unit	Mooring
Water Depth	m	106.8
Length	m	350
Diameter	m	0.12
EA	N	3.538991012E10
Density	kg/m <sup>3</sup>	8841.9413
Normal C <sub>D</sub>		1
Normal C <sub>M</sub>		2
Axial C <sub>D</sub>		0
Axial C <sub>M</sub>		1

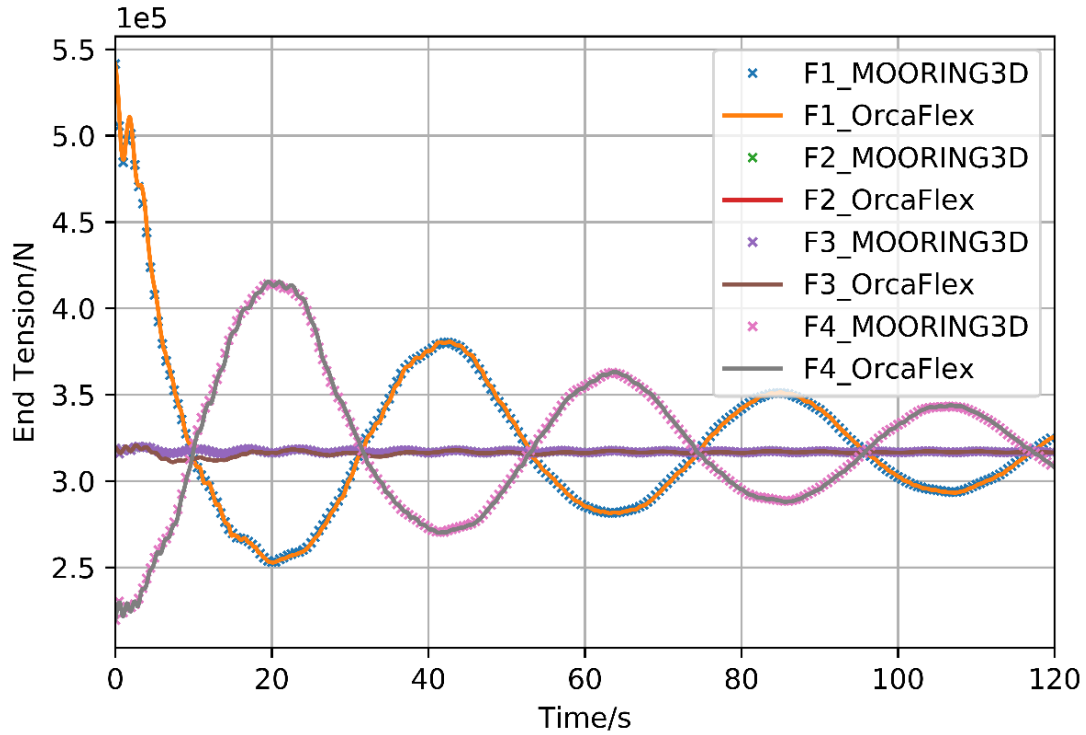


Fig. 2 Tension comparison between MOORING3D and OrcaFlex (Line1 – Line4)

The test is first simulated in the commercial software OrcaFlex. A free-decay test is used to generate the motion of the buoy and the motion of the four mooring lines' fairleads. The initial displacement of the buoy is  $-8$  m in  $x$  direction. The trajectories of four fairleads are used as the displacement inputs for the MOORING3D code to simulate a prescribed-motion test. The mooring lines used in the prescribed-motion test are the same as the ones used in OrcaFlex. Both the OrcaFlex and MOORING3D simulations were performed using 35 equally spaced elements along each mooring line.

By comparing the tangential tensions (from F1 to F4) at the top of each mooring line (from Line1 to Line4) computed by OrcaFlex and MOORING3D (Fig. 2), it can be verified that the MOORING3D code is able to simulate the dynamic responses of mooring lines with similar accuracy to OrcaFlex.

To demonstrate that the time interval of 0.1 second is sufficient for providing accurate simulation, tests with time increment of 0.01s and 0.2s are also conducted for comparison (Fig. 3). It is seen that the change of time interval has no effect on the final results, which means that the time interval of 0.1s is able to provide accurate estimation of the dynamic responses of the mooring line system.

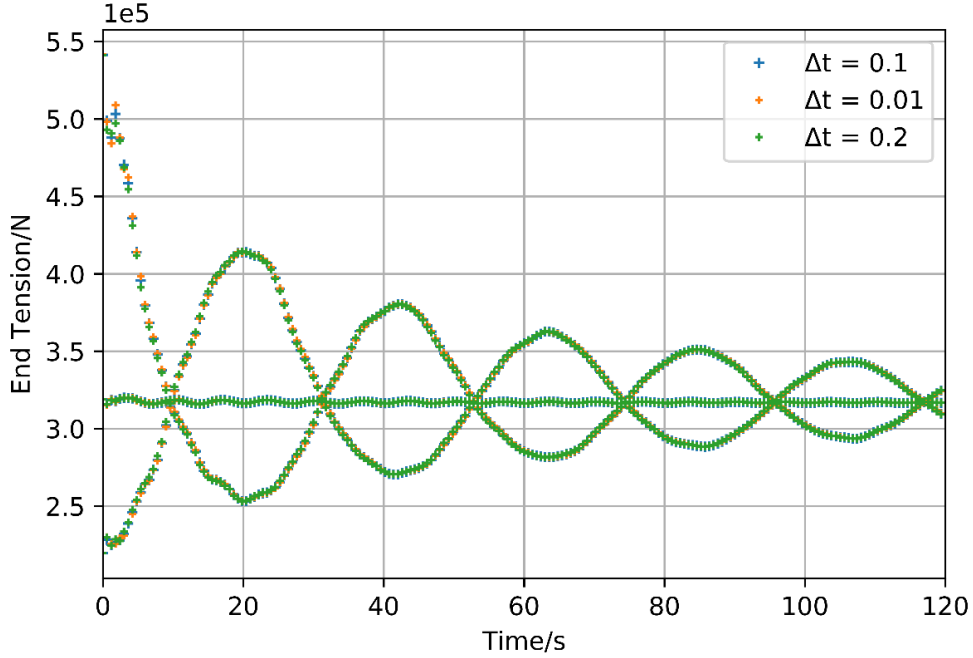


Fig. 3 Tension comparison between different time intervals (Line1 – Line4)

## 2.2 Computational Fluid Dynamics (CFD)

The flow field around the buoy is computed by solving the unsteady incompressible Navier-Stokes equations with the finite-analytic method (Pontaza *et al.* 2005, Chen *et al.* 2013, Chen and Chen 2016). Large eddy simulation (LES) turbulence model, which applies volume-averaging Navier-Stokes equation, is used to simulate the turbulence.

$$\frac{\partial \bar{u}_i}{\partial x_i} = 0 \quad (16)$$

$$\frac{\partial \bar{u}_i}{\partial t} + \frac{\partial}{\partial x_j} (\bar{u}_i \bar{u}_j) = -\frac{1}{\rho} \frac{\partial \bar{p}}{\partial x_i} + \nu \frac{\partial^2 \bar{u}_i}{\partial x_i \partial x_j} - \frac{\partial \tau_{ij}}{\partial x_i} \quad (17)$$

Eqs. (16) and (17) are the differential equation used by LES method.  $\tau_{ij}$  is the subgrid stress, which is determined by eddy-viscosity  $\nu_t$ . Smagorinsky's subgrid-scale turbulence model is utilized to estimate  $\nu_t$  (Eq. (18) to Eq. (22)).

$$\tau_{ij} = \bar{u}_i \bar{u}_j - \bar{u}_i \bar{u}_j \quad (18)$$

$$\tau_{ij} = -2\nu_t S_{ij} \quad (19)$$

$$\nu_t = (C_S \Delta)^2 \sqrt{2S_{ij} S_{ij}} \quad (20)$$

$$S_{ij} = \frac{1}{2} \left( \frac{\partial \bar{u}_i}{\partial x_j} + \frac{\partial \bar{u}_j}{\partial x_i} \right) \quad (21)$$

$$\Delta = (\Delta_x \Delta_y \Delta_z)^{1/3} \quad (22)$$

where  $S_{ij}$  is the local strain tensor.  $C_S = 0.1$  is the Smagorinsky's coefficient.  $\Delta$  is a filter width which filters out any vorticity smaller than it.

To best describe the motions of each subdomain of the fluid, an overset grid approach by Suhs and Tramel (1991) is used. With overset grid method, information among adjacent subdomains is transferred by overlapped common region between both borders.

The overset grid system for the buoy is shown in Figs. 4 and 5. The grid parameters are normalized by the characteristic length  $D$ , which is the outer diameter of the buoy. The total fluid domain size ranges from  $-5 \leq x/D \leq 12$ ,  $-5 \leq y/D \leq 5$  and  $-6.28235 \leq z/D \leq 0$ . There are a total of 7 computational blocks, including 5 near buoy cylindrical columns with 521,633 grid points and 2 rectangular blocks describing the far field of the fluid domain. The total number of the grid points is 1,223,378. With regard to the global coordinate system, x-axis stands for the incoming flow direction, y-axis is the cross-flow direction, and z-axis is the axial direction of the buoy.

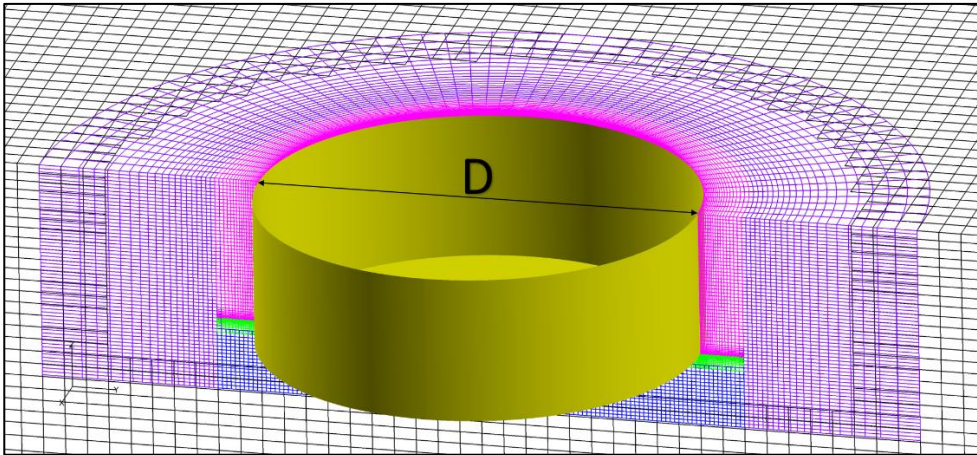


Fig. 4 Grids near the buoy model

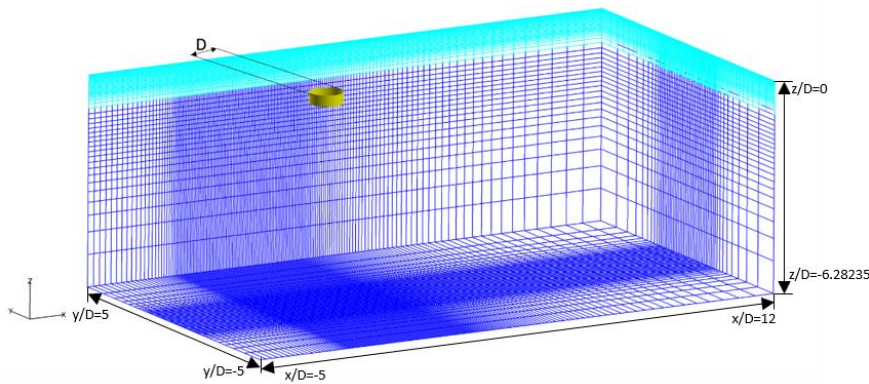


Fig. 5 Background grids and computational domain

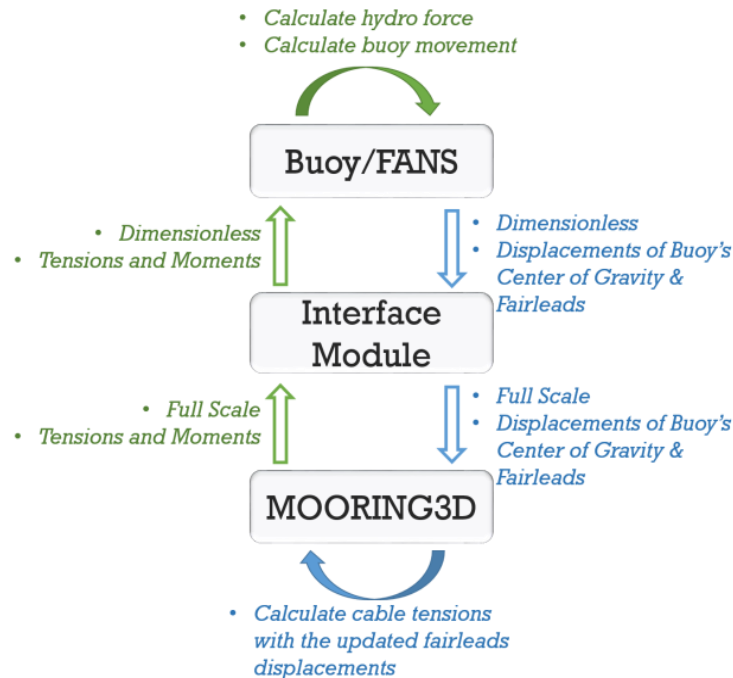


Fig. 6 Interaction between the three modules

### 2.3 Interface module

By using the MOORING3D module and FANS module, we are able to simulate the hydrodynamic behaviors of both the buoy model and mooring system. An interface module was established as a transmission channel to exchange the essential information between the FANS code and MOORING3D code. The general function and procedure for the whole simulation is demonstrated in Fig. 6.

At the beginning of each time step, the FANS code first updates the flow field and the hydrodynamic response of the buoy. The calculation is based on the updated information obtained from the last time step. The response of the buoy is calculated based on the updated total forces. The total external forces on the buoy are obtained by combining the hydro forces with the mooring lines' tensions, which are transferred from the MOORING3D module by means of the Interface module.

Being attached to the fairleads on the buoy, the mooring lines are forced to move at the same time. The motion of the fairleads is transferred from the FANS module to the MOORING3D module through the Interface module. The updated displacements for the mooring lines reversely affect the response of the buoy by exerting new external tensions and moments on the buoy.

In the coupled FANS/MOORING3D simulations, the Interface module is responsible for transferring the updated displacement of the buoy to the MOORING3D module as an input, and transferring the tensions and moments caused by the new displacement back to the FANS code as an external effect on the buoy. As all the parameters in the FANS module are dimensionless, the

Interface module is designed to normalize the input for the MOORING3D code and dimensionalize the input for the FANS code.

### 3. Numerical simulation

#### 3.1 Free-decay test

##### 3.1.1 Experimental set-up

To calibrate the dynamic characteristics of the CALM buoy system established by the coupled code, a free-decay model test conducted in the Offshore Engineering Basin at the Institute for Marine Dynamics in Canada by Ryu *et al.* (2006) has been replicated with the coupled code and OrcaFlex separately. The results from the coupled code and OrcaFlex are compared with the model test data to verify that the model established in the coupled code has the same hydrodynamic characteristics with the one in the model test.

The parameters of the prototype buoy are listed in Table 2. To facilitate a direct comparison with the model test data, numerical simulations were performed for the model-scale CALM buoy system. The scale ratio for the length of model test is  $\lambda = \frac{L_F}{L_M} = 35.6$ . As the model test in the wave basin follows the Froude similarity scaling law, the corresponding scale ratio for the velocity becomes  $\frac{U_F}{U_M} = \sqrt{\lambda} = \sqrt{35.6}$ . The time in the simulation is scaled with a ratio of  $\frac{T_F}{T_M} = \sqrt{\lambda} = \sqrt{35.6}$ .

Due to the limitation of experimental water depth, Ryu *et al.* (2006) used truncated mooring method in the model test to replicate equivalent dynamic behaviors of the prototype mooring system. The full-scale parameters of the mooring lines employed in the model test is presented in Table 3. To facilitate a direct comparison with the model test results, the parameters of the mooring lines in the coupled code and OrcaFlex are the same as the ones in the model test. Fig. 7 present the 3D overview of the experimental configuration.

Table 2 Buoy's parameters

Parameter	Unit	Value
Model Test Scale		35.6
Water Depth	m	106.8
Buoy Hull Diameter	m	17.0
Buoy Height	m	7.65
Draft	m	5.65
Weight in Air	ton	878.6
KG	m	3.4
Buoy Total $R_{xx}$	m	4.39
Buoy Total $R_{yy}$	m	4.39

Table 3 Parameters of the mooring lines in the model test (full-scale)

	Unit	Mooring
Length	m	133.3
Wet Weight	kg/m	3
Diameter	mm	30
EA	metric tons	1963
Pretension	metric tons	150

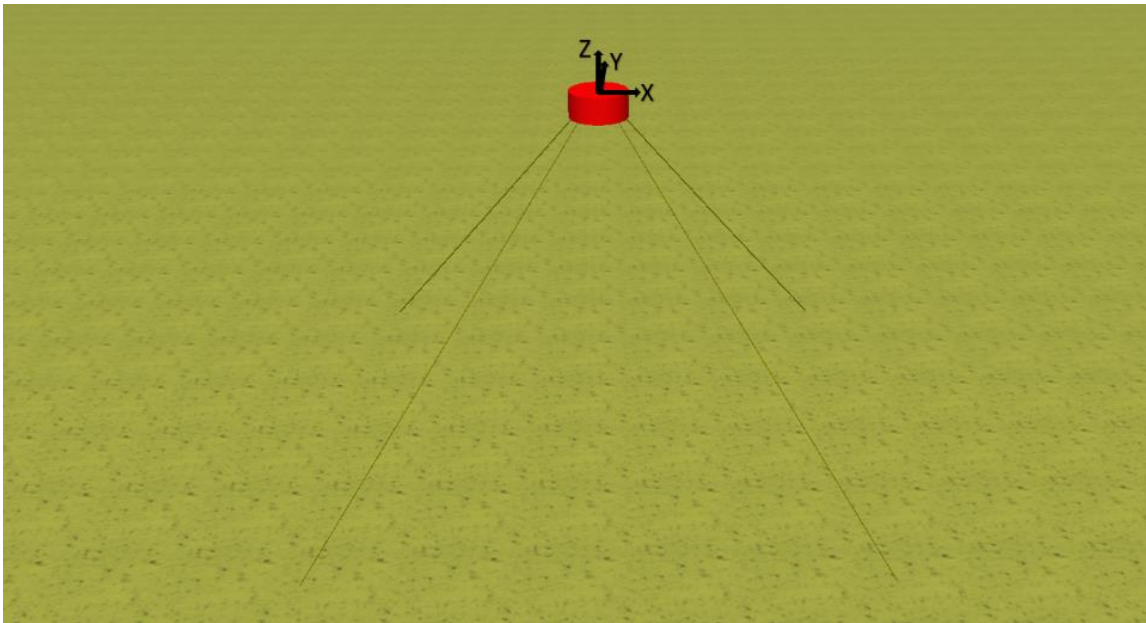


Fig. 7 3D overview of mooring lines' configuration

### 3.1.2 Simulation results

Fig. 8 compares the surge displacements of the buoy model obtained from the three tests. The hydrodynamic coefficients of the buoy in OrcaFlex is shown in Table 4. For the numerical methods, the simulation time increment used in the free-decay test is 0.1s in prototype scale. As the model test only provides the results from 0 to 120s in the full-scale, the number of iteration steps is set to be 1200.

Fig. 9 illustrates the 2D and 3D z-vorticity patterns in free-decay test at simulation time steps of 200, 500 and 1000, which correspond to full-scale time of 20s, 50s and 100s. The 2D contours is obtained on the plane of  $z/D = -0.2$ , which is 3.4 meters below the free surface.

Compared with the surge displacement in Fig. 8, at the time step of 200, the buoy reaches the leftmost (minimum x) position within one period. It is seen in Fig. 9(a) that the vortex is mainly

located on the positive side of the buoy, which is an accumulative consequence of unidirectional surge motion in previous time steps. At the time step of 500, the buoy reaches the rightmost (maximum  $x$ ) position. It is clear that new vortex has been generated on the negative side of the buoy. Instead of dissipating instantly, the vortex generated in the previous oscillation period still exists. The vortices on both sides of the buoy tend to drift further in opposite direction, which is depicted in Fig. 9(c). This phenomenon can be explained with a 3D view of the vortex generation in  $z$  direction. Due to the shallow draft of the buoy, a large amount of vortex appears at the bottom corner of the buoy. The vortex is pushed upward by the motion of the buoy, which strengthens the vortex on the upper layer.

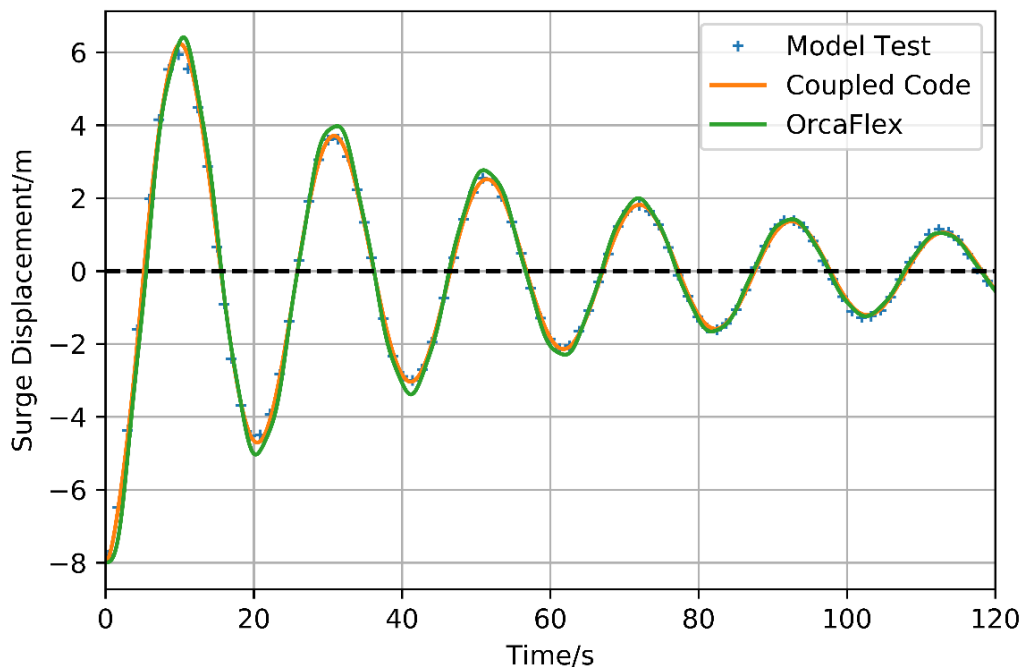


Fig. 8 Surge comparison in free-decay test

Table 4 Buoy's hydrodynamic coefficients in OrcaFlex

	Unit	New Mooring
Normal Drag Coefficient		0.49
Axial Drag Coefficient		7
Normal Added Mass Coefficient		0.71
Axial Added Mass Coefficient		1

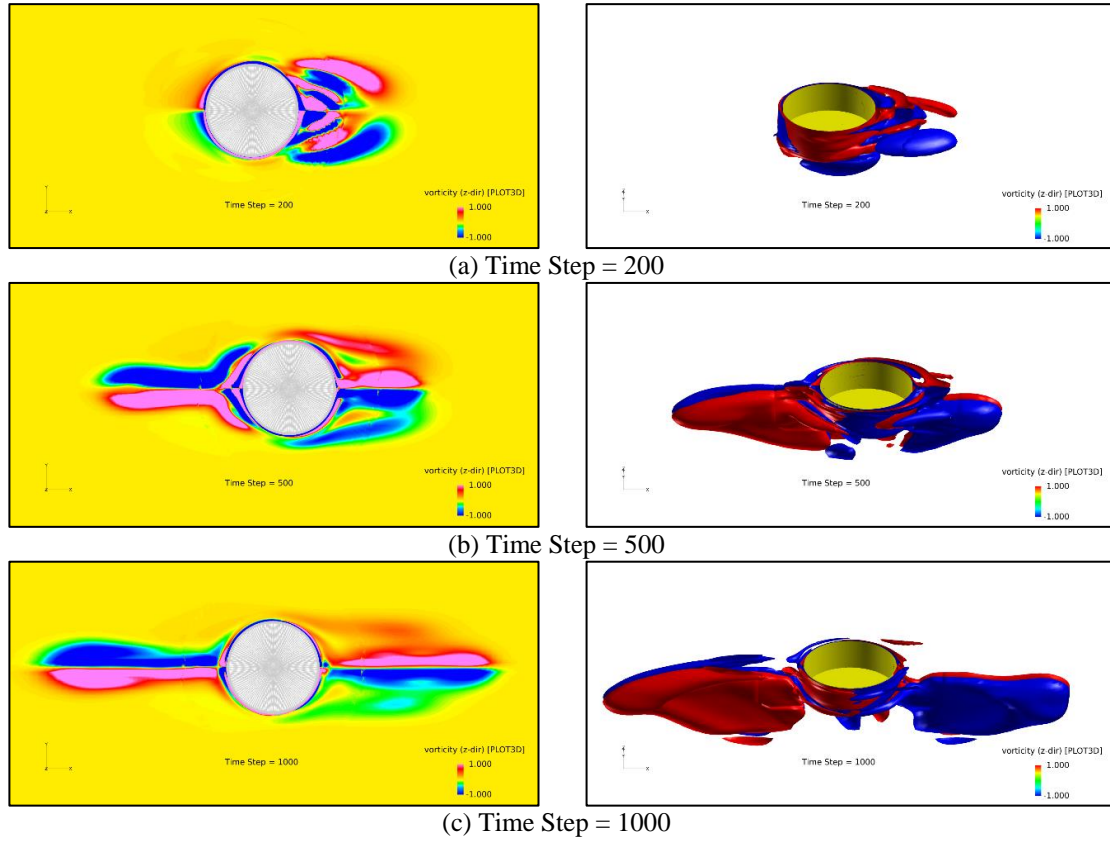


Fig. 9 2D and 3D vorticity contours in z direction

From Fig. 8, it can be seen that the displacements of the CALM buoy model are in a good agreement between the model test and the two numerical methods. The CALM buoy system model used in the coupled method is calibrated successfully with the same hydrodynamic behavior, which proves that the coupled code is able to predict the hydrodynamic response of the CALM buoy system accurately and the model can be used for further study. To ensure the results are parameter-independent, a grid refinement study and a time interval study are conducted.

### 3.1.3 Parametric study

A grid refinement study is conducted with different resolutions of grids in the fluid domain near the buoy model. The resolution of the grid is controlled by two parameters,  $\Delta\theta$  and  $\Delta r$ , which are illustrated in Fig. 10.

By adjusting  $\Delta\theta$  and  $\Delta r$ , the resolution of the grid is changed. Table 5 shows the detailed information about the grid refinement test. The number of grid points used in the calibration test is the one with medium resolution. The CPU time for each condition is also included in Table 5.

The comparison of surge displacement in the three cases is shown in Fig. 11. It is seen that the change of grid resolution does not have much effect on the final result, which means that estimation provided by the coupled code is grid-independent and the medium grid provides adequate resolution for present applications.

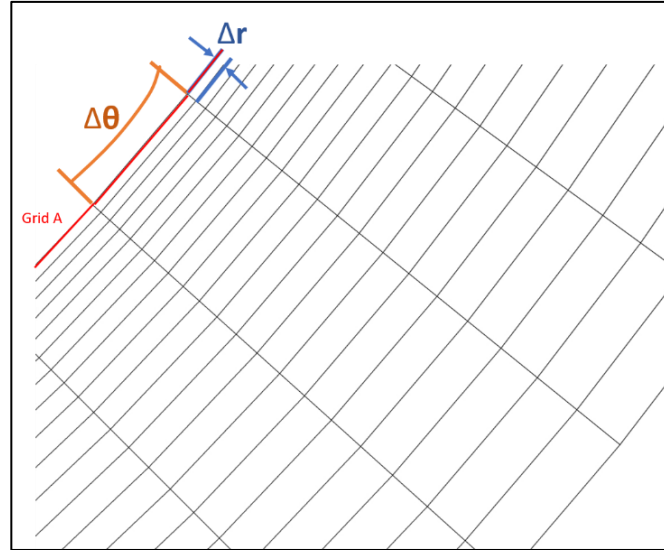


Fig. 10 Zoom-in view of the grid

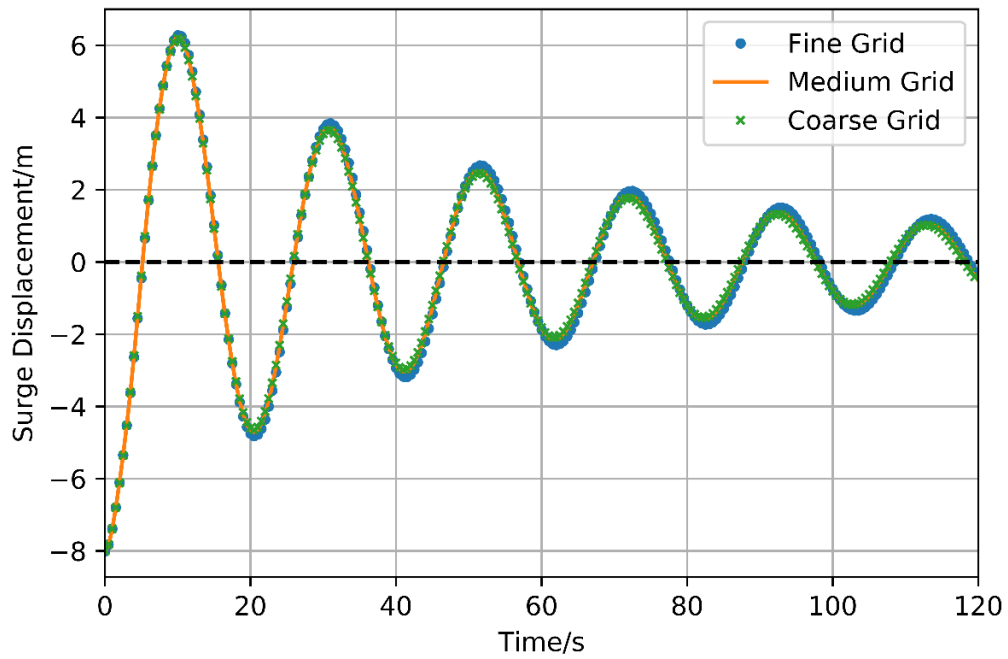


Fig. 11 Comparison of surge displacement with different grid resolution

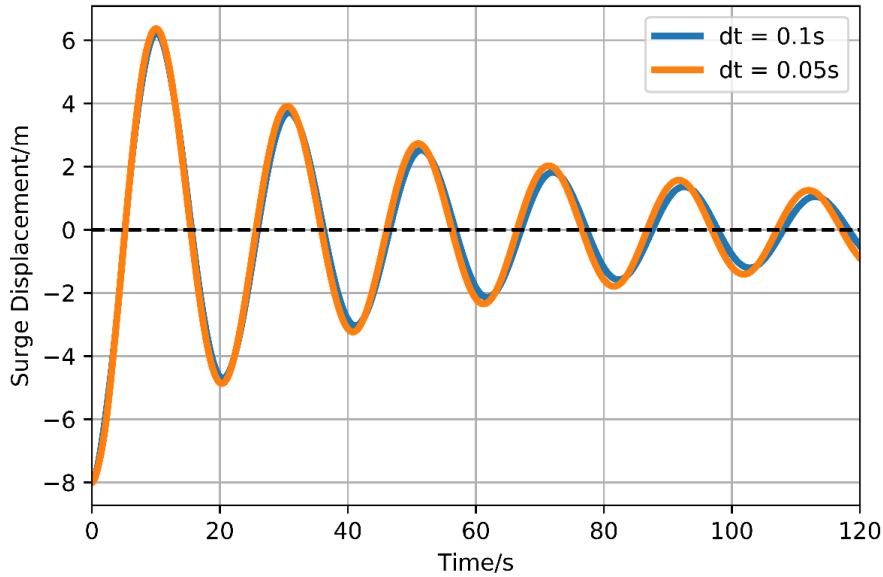


Fig. 12 Comparison of surge displacement with different time intervals

Table 5 Parameters for grid refinement test

	$\Delta\theta$	$\Delta r/D$	Near Body Number	Off Body Number	CPU Time (sec/time step)
Fine Grid	2.25°	0.001	722385	1424130	13.80258
Medium Grid	3.0°	0.002	521633	1223378	13.49448
Coarse Grid	4.5°	0.002	359113	1060858	12.45798

Time interval study is also conducted to confirm that the results are independent of simulation time increment for each time step. The time step size used for calibration free-decay test is 0.1s. Numerical simulation with time interval of 0.05s is conducted for comparison. The comparison of surge displacement in the two cases is shown in Fig. 12. From the picture it is seen that the change of time increment does not have much effect on the final results, which means the time interval of 0.1s for each time step is able to provide accurate estimation for present simulation.

### 3.2 Uniform current test

#### 3.2.1 Experimental set-up

After successful calibration of the numerical CALM buoy system model, the coupled FANS/MOORING3D code is employed to predict the hydrodynamic responses of the buoy model under a constant uniform current condition. The model used in this test is the same as the one in the free-decay test.

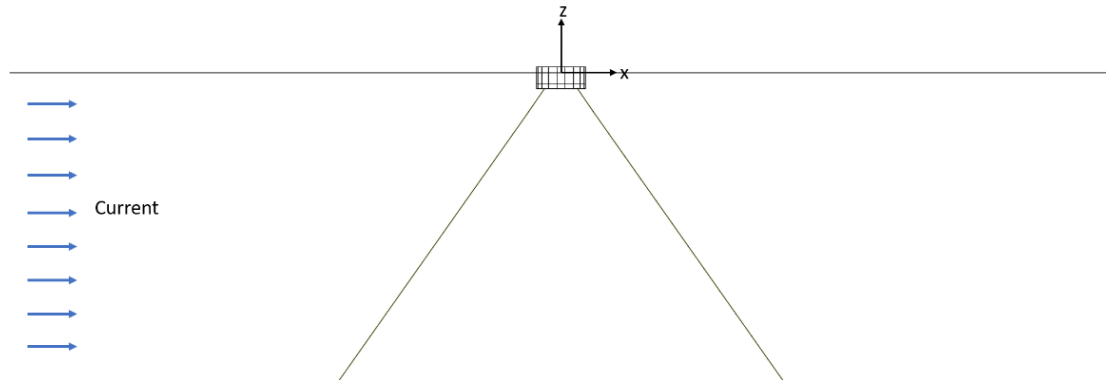


Fig. 13 Side view of the uniform current test

The gravity center of the buoy is kept static at the origin of the global coordinate on x-y plane. Like what is shown in Fig. 13, a steady current with uniform velocity comes from the far field in x direction.

### 3.2.2 Test with current velocity of 1m/s

A comparative study is conducted between the coupled FANS/MOORING3D method and OrcaFlex with full-scale current velocity of 1 m/s. The number of calculation time steps is 20000, with a full-scale time interval of 0.1s. To verify the accuracy of the result simulated by the coupled code, a same case is also conducted with OrcaFlex. The parameters and input information applied in both simulations are identical.

Fig. 14 shows the comparison between OrcaFlex and the coupled code in terms of surge and sway displacements during the time from 0 to 2000 s. For the surge displacement, as the coupled method considers the impulsive start of the CALM buoy motion, compared to the amplitude of oscillation in OrcaFlex, the initial amplitude in the coupled code is much larger. The surge motion in OrcaFlex reaches steady-state condition after 200 s, while the surge displacement in the coupled method oscillates around an equilibrium position, which is also a little bit farther away from the origin point than the stationary position in OrcaFlex. For the comparison of sway displacement, it is seen that compared to the simulation with the coupled code, there is no motion in y direction in OrcaFlex. Based on the results from the coupled method, the buoy oscillates irregularly in both positive and negative directions of y axis.

Fig. 15 compares xy-trajectories of the buoy estimated by the coupled code and OrcaFlex. Compared to the pure surge motion only in x direction in OrcaFlex, there exist oscillations in y direction according to the result from the coupled method. Additionally, it is shown that the amplitude of the sway motion is much smaller than that of the surge motion.

Fig. 16 depicts the comparison between the coupled code and OrcaFlex in terms of the total force and its component forces (i.e., hydro force and tension from mooring lines) exerted on the buoy model in both surge and sway directions. From the picture, it is seen that the differences between the two methods in the force terms are the same as those in the motion terms in Fig. 14.

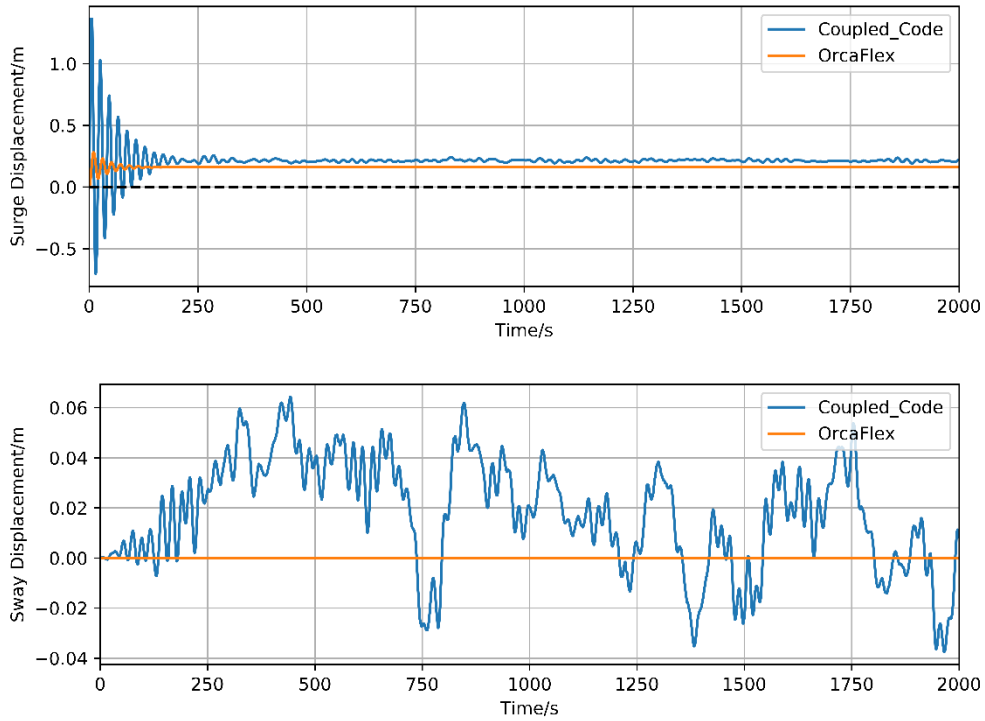


Fig. 14 Comparison of surge and sway displacements with current velocity = 1 m/s

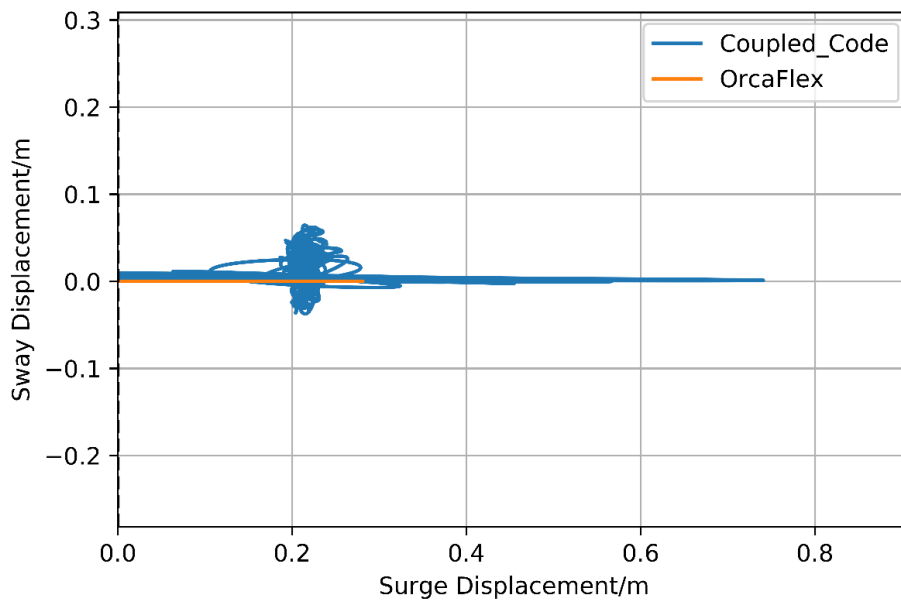


Fig. 15 Comparison of xy-trajectories

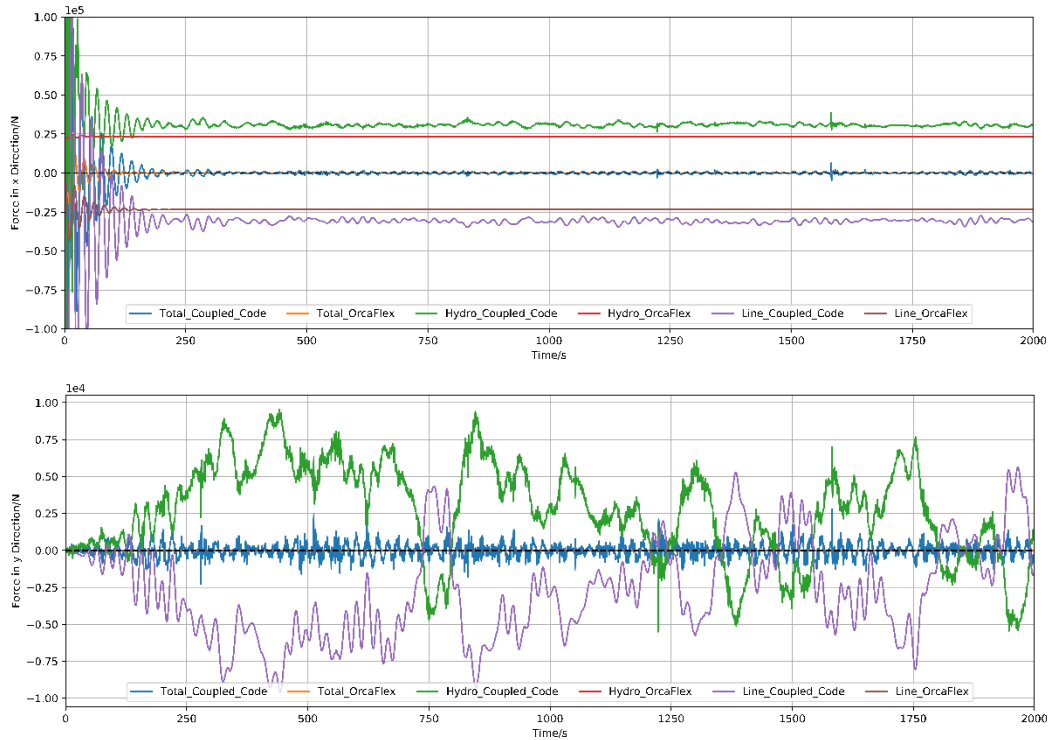


Fig. 16 Comparison of forces on the buoy in x and y directions

The differences in the forces and displacements predicted by OrcaFlex and the coupled code can be explained by Fig. 17, which shows the 2D and 3D vorticity patterns in z direction on the surface of  $z = -3.4\text{m}$ . The selected full-scale time instants are 100s, 200s and 1000s, respectively, which stand for three typical stages of the response of the buoy based on Figs. 14 and 16. Due to the unsteady vortex shedding throughout the process, it is reasonable that the displacements and forces of the buoy continue to oscillate about the equilibrium position. As the effect of vortex is not taken into account in OrcaFlex, the estimated buoy motion and forces are different from the ones predicted by the coupled method, especially in the crossflow direction.

### 3.2.3 Parametric study of current velocities

Based on the results from the uniform current case, it is verified that the coupled method is able to resolve the viscous effect on the hydrodynamic behavior of the CALM buoy system. Additional cases with higher uniform current speeds are conducted to study the vortex-induced motion of the CALM buoy system.

The CALM buoy system model is the same as the one used in 3.2.2. The direction of the incoming uniform current is the same as that shown in Fig. 13. To study the correlation between vortex-induced motion of the buoy and the current speed, current velocities of 1 m/s, 2 m/s, 3 m/s and 4 m/s are applied for different cases.

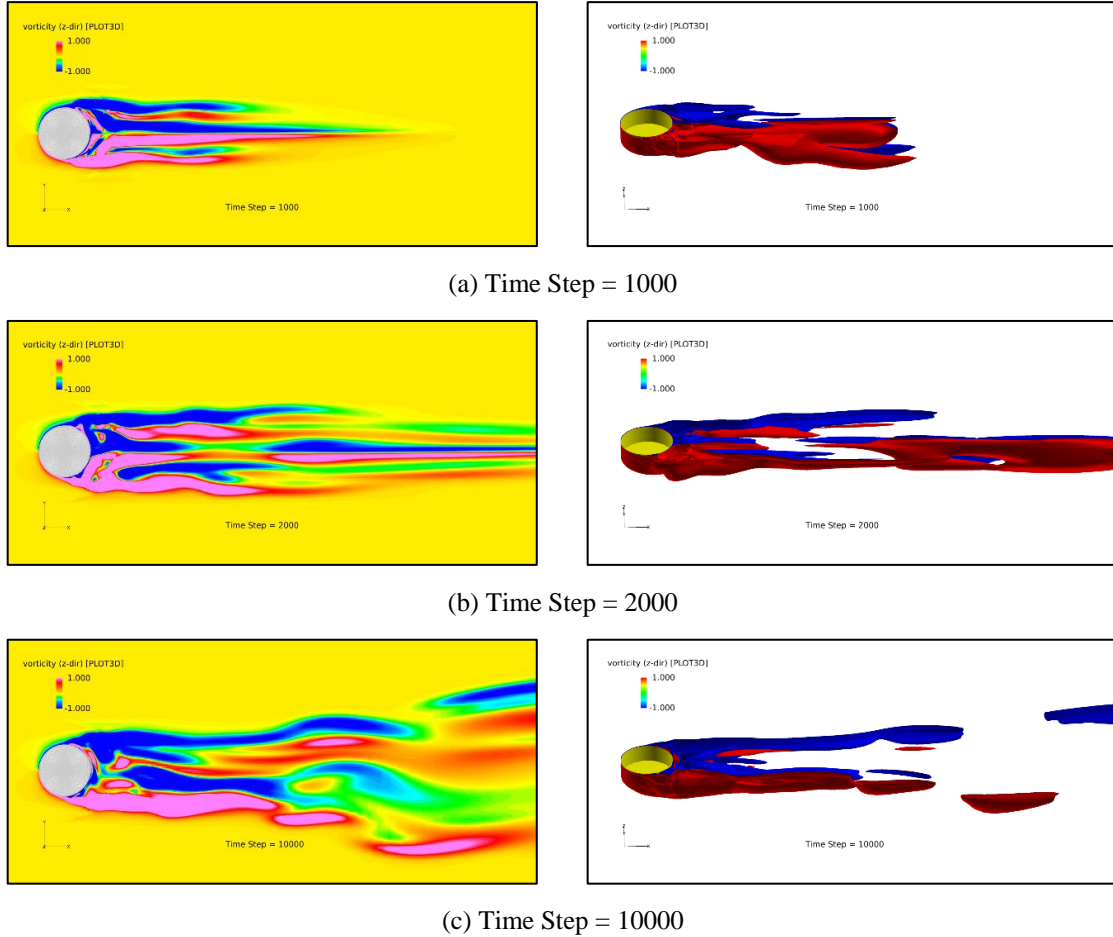


Fig. 17 2D and 3D vorticity contours in z direction

To ensure proper resolution of the vortex shedding process and vortex-induced motions of the CALM buoy, the time step sizes are adjusted for each different current velocities. Table 6 shows the corresponding time interval for each current velocity. The simulation time is 2000s in prototype scale.

Table 6 Current velocities and corresponding time interval

Current Velocity (m/s)	Reduced Velocity	Time Interval (s)
1	1.208823529	0.1
2	2.417647059	0.05
3	3.626470588	0.02
4	4.835294118	0.02

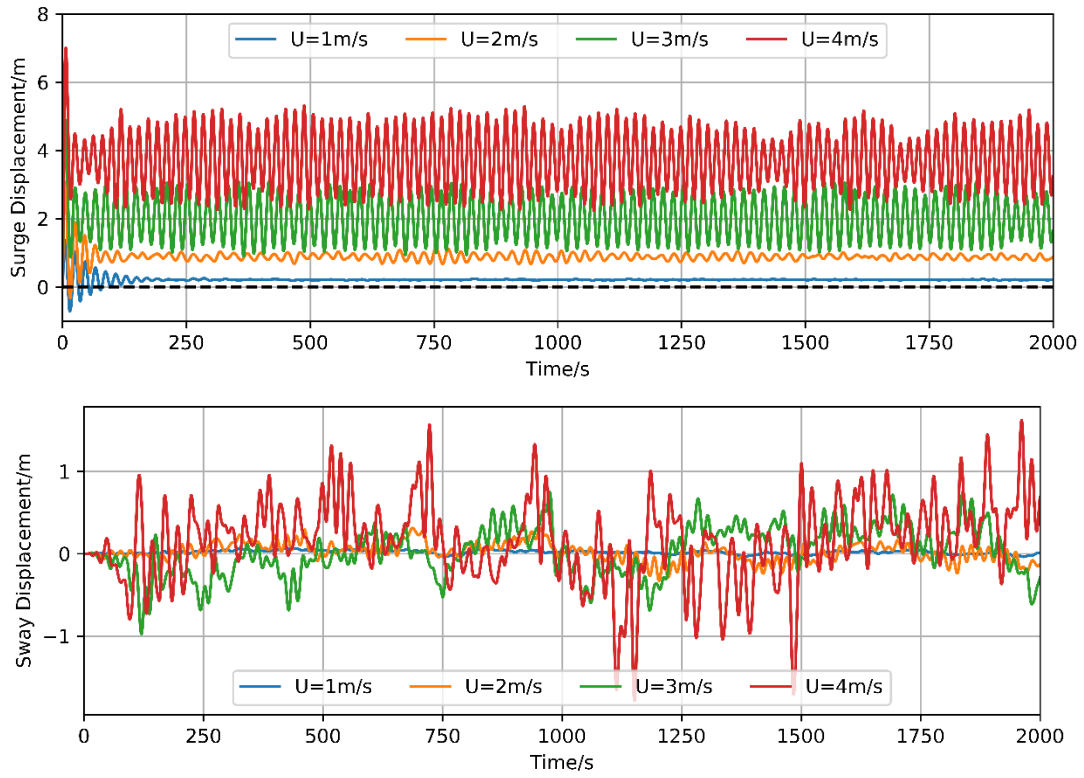


Fig. 18 Comparison of surge and sway displacements under different uniform current velocities

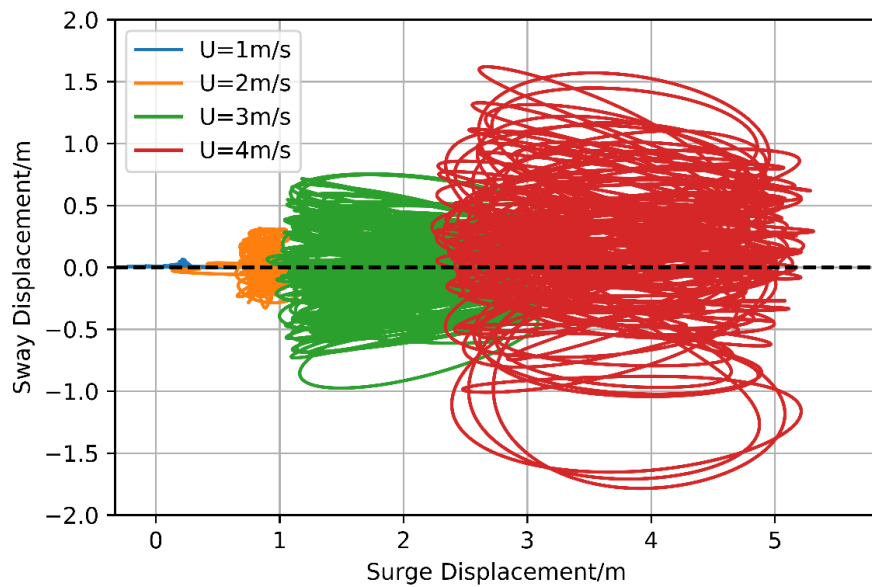


Fig. 19 Comparison of xy-trajectories under different uniform current velocities

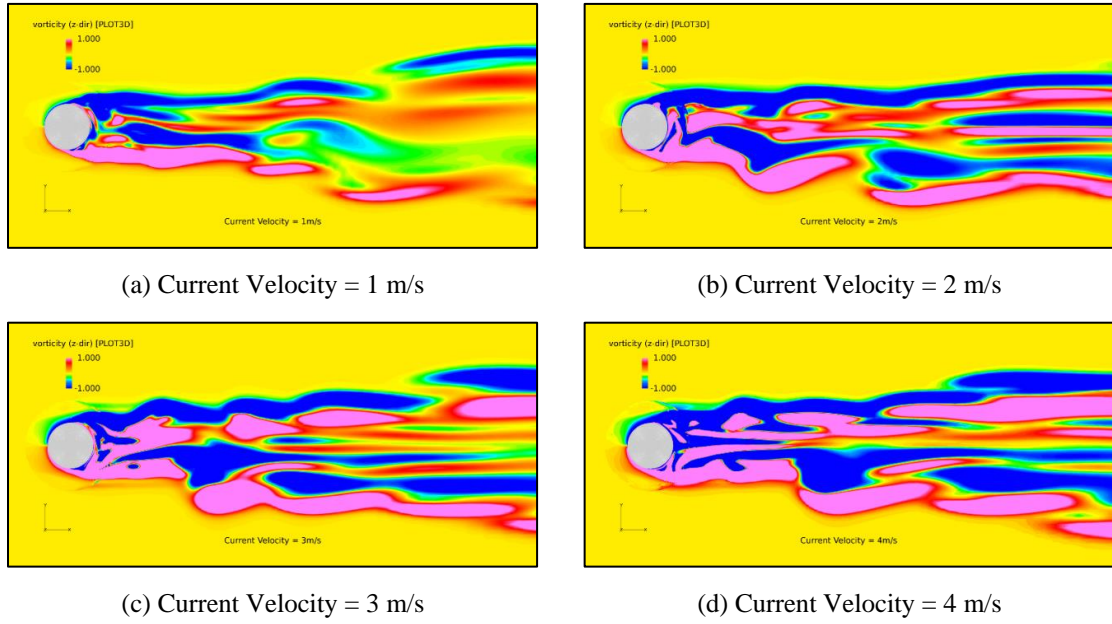


Fig. 20 Vorticity contours with different current velocities at  $t = 1000s$

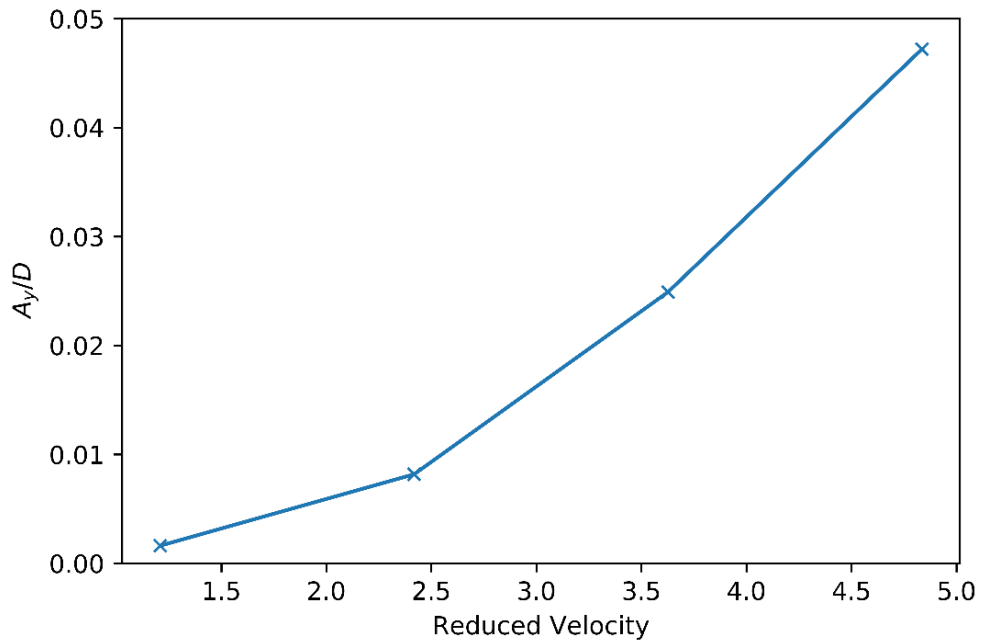


Fig. 21 VIM response of buoy

Figs. 18 and 19 show the comparison of the buoy displacements in x and y directions under the condition of different current velocities. With the increase of the current velocity, the amplitudes of the oscillations in both x and y directions increase as well. Due to the drag forces induced by the ocean current, the equilibrium positions around which the buoy oscillates in x direction also increases with the increase of current velocities.

The displacement of buoy in y direction is mainly caused by the generation of vortex and vortex shedding. Fig. 20 compares the vortex contours in z direction under different current velocities at full-scale time instant of 1000s. The position of the fluid surface is  $z = -3.4$  m. It is seen that the effect of vortex and vortex shedding increases with the increment of current velocity. The vorticity pattern in z-direction becomes more complicated as the current velocity increases. It can be inferred that the amplitudes of oscillations in surge and sway displacements are directly related to the strength of vortices generated by uniform currents.

Fig. 21 illustrates the relation between the amplitude of vortex-induced motion and the current velocity. From the picture it is seen that the vortex-induced motion (VIM) responses of the buoy is below the significant amplitude (0.15D) when the reduced velocity is smaller than 5, which means that under the condition of typical ocean current velocities, the VIM response of the buoy is small compared to the size of the buoy.

#### 4. Conclusions

A coupled Finite-Analytic Navier-Stokes (FANS) and MOORING3D method is employed to simulate the hydrodynamic behaviors of CALM buoy system in this study. A free-decay model test was utilized to calibrate the numerical model. A comparative study with 1 m/s uniform current velocity was conducted between the coupled code and OrcaFlex to verify the accuracy of the CFD method. It is shown that the contribution of vortex shedding can be successfully estimated with the coupled method. Tests with different uniform current speeds were also conducted to study the VIM responses of the CALM buoy system. The result shows that the hydrodynamic behavior of the buoy is affected by the vorticity, although the response induced by VIM is small for the buoy model under typical current speeds.

In summary, a coupled FANS/MOORING3D method has been developed to simulate the hydrodynamic behavior of the CALM buoy system for a wide range of ocean current speeds. The method will be further developed in the aspect of simulations with more complicated geometries and environmental conditions.

#### Acknowledgments

The authors would like to thank the Texas A&M University High Performance Research Computing (HPRC) Center for providing the computing resources.

#### References

Bunnik, T., de Boer, G., Cozijn, J., van der Cammen, J., van Haafden, E. and ter Brake, E. (2002), "Coupled mooring analysis and large scale model tests on a deepwater calm buoy in mild wave conditions",

- Proceedings of the 21st International Conference on Offshore Mechanics and Arctic Engineering*, Oslo, Norway, June.
- Chen, C.R. and Chen, H.C. (2016), "Simulation of vortex-induced motions of a deep draft semi-submersible in current", *Ocean Eng.*, **118**, 107-116.
- Chen, H.C., Chen, C.R. and Huang, K. (2013), "Cfd simulation of vortex-induced and wake-induced vibrations of dual vertical risers", *Proceedings of the The 23rd International Offshore and Polar Engineering Conference*, Anchorage, Alaska, June.
- Chen, X. (2002), "Studies on dynamic interaction between deep-water floating structures and their mooring/tendon systems", Ph.D. Dissertation; Texas A & M University, College Station, Texas, U.S.A.
- Cozijn, J. and Bunnik, T. (2004), "Coupled mooring analysis for a deep water calm buoy", *Proceedings of the 23rd International Conference on Offshore Mechanics and Arctic Engineering*, Vancouver, British Columbia, Canada, June.
- Duggal, A. and Ryu, S. (2005), "The dynamics of deepwater offloading buoys", *Fluid Struct. Interact. Moving Bound. Probl.*, **84**, 269-278.
- Garrett, D.L. (1982), "Dynamic analysis of slender rods", *J. Energy Resour.*, **104**(4), 302-306.
- Gu, H., Chen, H.C. and Zhao, L. (2017), "Coupled mooring analysis of a calm buoy by a cfd approach", *Proceedings of the the 27th International Ocean and Polar Engineering Conference*, San Francisco, California, USA, June.
- Huang, Z., Santala, M., Wang, H., Yung, T., Kan, W. and Sandstrom, R. (2005), "Component approach for confident predictions of deepwater calm buoy coupled motions: Part 1—philosophy", *Proceedings of the 24th International Conference on Offshore Mechanics and Arctic Engineering*, Halkidiki, Greece, June.
- Kang, Y., Sun, L., Kang, Z. and Chai, S. (2014), "Coupled analysis of fpso and calm buoy offloading system in west africa", *Proceedings of the 33rd International Conference on Ocean, Offshore and Arctic Engineering*, San Francisco, California, USA, June.
- Le Cunff, C., Ryu, S., Duggal, A., Ricbourg, C., Heurtier, J., Heyl, C., Liu, Y. and Beauclair, O. (2007), "Derivation of calm buoy coupled motion raos in frequency domain and experimental validation", *Proceedings of the 17th International Offshore and Polar Engineering Conference*, Lisbon, Portugal, July.
- Lindahl, J. and Sjoberg, A. (1983), "Dynamic analysis of mooring cables", Research Report No. A:9; Chalmers Univ. Technology, Goteborg.
- Monroy, C., Ducrozet, G., Bonnefoy, F., Babarit, A., Gentaz, L. and Ferrant, P. (2011), "Rans simulations of calm buoy in regular and irregular seas using swense method", *Int. J. Offshore Polar Eng.*, **21**(4), 264-271.
- Pontaza, J., Chen, C. and Chen, H. (2005), "Simulation of high reynolds number flow past arrays of circular cylinders undergoing vortex-induced vibrations", *Proceedings of the The 15th International Offshore and Polar Engineering Conference*, Seoul, Korea, June.
- Ricbourg, C., Berhault, C., Camhi, A., Lécuyer, B. and Marcer, R. (2006), "Numerical and experimental investigations on deepwater calm buoys hydrodynamics loads", *Proceedings of the 2006 Offshore Technology Conference*, Houston, Texas, U.S.A., May.
- Ryu, S., Duggal, A.S., Heyl, C.N. and Liu, Y. (2006), "Prediction of deepwater oil offloading buoy response and experimental validation", *Int. Soc. Offshore Polar Engineers*, **16**(4), 290-296.
- Sagrilo, L., Siqueira, M., Ellwanger, G., Lima, E., Ferreira, M. and Mourelle, M. J. A. o. r. (2002), "A coupled approach for dynamic analysis of calm systems", *Appl. Ocean Res.*, **24**(1), 47-58.
- Salem, A.G., Ryu, S., Duggal, A.S. and Datla, R.V. (2012), "Linearization of quadratic drag to estimate calm buoy pitch motion in frequency-domain and experimental validation", *J. Offshore Mech. Arct. Eng.*, **134**(1), 011305.
- Suhs, N. and Tramel, R. (1991), "Pegsus 4.0 user's manual", Research Report No. ADA280608; Arnold Engineering Development Center Arnold AFB TN